Dalton Transactions

PAPER

Check for updates

Vibrational spectroscopy of dispersed $Re^{VII}O_x$ sites supported on monoclinic zirconia†

Chrysanthi Andriopoulou,[a] Theocharis Kentri[a] and Soghomon Boghosian ID *[a,b,c]

In situ Raman and FTIR spectra complemented by *in situ* Raman/^{18}O isotope labelling are exploited for deciphering the structural properties and configurations of the $(ReO_x)_n$ phase dispersed on monoclinic ZrO_2 at temperatures of 120–400 °C under oxidative dehydration conditions and coverages in the range of 0.71–3.7 Re nm^{-2}. The dispersed $(ReO_x)_n$ phase is heterogeneous, consisting of three distinct structural units: (a) Species-I with mono-oxo termination O=Re(−O−Zr)$_m$ (Re=O mode at 993–1005 cm^{-1}); (b) Species-IIa with di-oxo termination (O=)$_2$Re(−O−Zr)$_{m-1}$ (symmetric stretching mode at 987–998 cm^{-1}); and (c) Species-IIb with di-oxo termination (O=)$_2$Re(−O−Zr)$_u$ (symmetric stretching mode at 982–991 cm^{-1}); all terminal stretching modes undergo blue shifts with increasing coverage. With increasing temperature, a reversible temperature-dependent Species-IIa ↔ Species-I transformation is evidenced. At low coverages, below 1 Re nm^{-2}, isolated species prevail; at 400 °C the mono-oxo O=Re(−O−Zr)$_m$ Species-I is the majority species, the di-oxo Species-IIa occurs in significant proportion and di-oxo Species-IIb is in the minority. At coverage ≥1.3 Re nm^{-2}, at 400 °C the di-oxo Species-IIa prevails clearly over mono-oxo Species-I. Below 80 °C and at a low coverage of 0.71 Re nm^{-2}, the occurrence of a fourth structural unit, Species-III taking on a tri-oxo configuration (symmetric stretching mode at 974 cm^{-1}) is evidenced. All temperature-dependent structural and configurational transformations are fully reversible and interpreted by mechanisms at the molecular level.

1. Introduction

Several technologically important catalytic reaction processes benefit from supported rhenium oxide catalysts. Pertinent paradigms of such processes include olefin metathesis over ReO_x/Al_2O_3,[1–3] selective catalytic oxidation of light alcohols over ReO_x supported on TiO_2 and SnO_2,[4] methanol conversion to dimexothymethane over ReO_x dispersed on TiO_2(anatase), ZrO_2 (monoclinic), SiO_2 and Al_2O_3,[5–8] as well as hydrodesulfurization and hydrodenitrogenation processes over ReO_x/Al_2O_3 catalysts.[9,10]

Diverging and often contradictory reports have been published in the literature of supported rhenia catalysts concerning the speciation and the molecular structure of the dispersed dehydrated $Re^{VII}O_x$ phase. Combined Raman and IR spectra recorded after cooling at 45 °C under dehydrated conditions were interpreted to suggest the existence of two distinct tri-oxo

(O=)$_3$–Re–O species on Al_2O_3, TiO_2 and ZrO_2 with relative amounts varied by surface coverage,[11] whereas the same group proposed the existence of one single tri-oxo (O=)$_3$–Re–O species based on Raman spectra obtained at room temperature after dehydration at 500 °C for 1 wt% Re_2O_7 on SiO_2, Al_2O_3, TiO_2 and ZrO_2.[12] Consistently with ref. 12, one single isolated species with tri-oxo termination configuration is proposed for ReO_x dispersed at surface densities of 0.3–2.2 Re nm^{-2} on TiO_2 and Al_2O_3 based on *in situ* Raman and FTIR spectroscopy under oxidative dehydrating conditions (at 400 °C and 300 °C, respectively).[13] Later, the same laboratory, based on an elegant study employing *in situ* Raman spectroscopy coupled with ^{18}O/^{16}O isotope exchange at 450 °C on one single sample (3 wt% Re_2O_7/ZrO_2) suggested the occurrence of a polymeric species with mono-oxo termination configuration.[14] Additionally, a theoretical (DFT and X-ray spectroscopy simulations) study combined with experimental work (XAFS, STEM, TPR, XPS) performed at room temperature after cooling under controlled conditions on one single sample (0.7 wt% Re on Al_2O_3) suggested the existence of isolated tri-oxo ReO_x.[15] Separately, the occurrence of two distinct di-oxo (O=)$_2$–Re(−O−)$_2$ species on Al_2O_3 has been convincingly shown following a sound experimental (*in situ* Raman coupled with ^{18}O/^{16}O exchange, *in situ* IR, UV-Vis, XANES) investigation combined with theoretical analysis (DFT).[16] *Operando* Raman studies

*[a]Department of Chemical Engineering, University of Patras, Patras, Greece.
E-mail: bogosian@chemeng.upatras.gr*
[b]Institute of Chemical Engineering Sciences, FORTH/ICE-HT, Patras, Greece
[c]School of Science and Technology, Hellenic Open University, GR-26335 Patras, Greece

have also provided evidence for heterogeneity of the dispersed ReO_x phase on TiO_2.[7,8] An *in situ* Raman spectroscopic study coupled with $^{18}O/^{16}O$ isotope exchange at 450 °C showed that a tri-oxo $(O{=})_3$–Re–O– configuration prevails on SiO_2.[17] A heterogeneity and an unprecedented reversible temperature-dependent evolution of prevailing structures and configurations (mono-oxo *vs.* di-oxo) has been established for the dispersed MoO_x, WO_x and ReO_x phases on TiO_2 by means of *in situ* molecular vibrational (Raman and FTIR) spectroscopy at temperatures of 175–430 °C.[18] Unlimited cycling between the mono-oxo configuration (prevalent at high temperature) and the di-oxo configuration (predominant at intermediate temperature) is feasible by appropriate temperature control and adequate sample exposure.[19] The extent of temperature dependence is connected to the support (TiO_2) surface hydroxylation as demonstrated by complementary Raman spectra in sealed cells under forced dehydrated conditions.[19] The dispersed ReO_x phase on TiO_2(P25) in the submomolayer 0.16–2.5 Re nm^{-2} range consists of a mono-oxo $O{=}Re(–O–Ti)_n$ species and a di-oxo $(O{=})_2Re(–O–Ti)_m$ species, in relative amounts that depend on temperature and coverage, as shown by means of *in situ* molecular vibrational (Raman and FTIR) spectroscopy complemented by $^{18}O/^{16}O$ isotope exchange and Raman spectra in sealed cells under forced dehydrated conditions.[20] The occurrence of a mono-oxo and a di-oxo species has also been demonstrated by means of *in situ* molecular vibrational spectroscopy (Raman and FTIR) coupled with $^{18}O/^{16}O$ exchange for the ReO_x phase dispersed on CeO_2.[21] An overview of selected reports on the molecular structure of dispersed ReO_x sites is contained in a recent review on vibrational spectroscopy of supported transition metal oxides.[22] Molecular vibrational spectroscopy is particularly suited for studying the transition metal oxide phases dispersed on oxide carriers since it can be applied in absence of long range order. Moreover, the combined use of Raman and FTIR spectroscopy, complemented also by isotope exchange provides a comprehensive approach that can differentiate amongst distinct molecular configurations exhibited by $(MO_x)_n$ sites (M = *e.g.* V, Mo, W, Nb, Re *etc.*).[22] A recently demonstrated neoteric concept of Raman spectroscopy of supported transition metal oxides in sealed cells under forced dehydrated conditions has also contributed in validating results obtained by *in situ* vibrational (Raman, IR) spectroscopies.[19,20,23,24]

In our view, the reasons for the controversy on the reported molecular structures of dispersed transition metal oxides in some pre-2015 reports are to be found in the deficiencies of the research strategies adopted in most of the pertinent investigations. Such deficiencies may include one or more of the following shortcomings: (i) studying only one type of vibrational spectra and/or not complementing the study with isotope exchange measurements; (ii) recording of vibrational spectra at room temperature after cooling; (iii) examining the structural properties of one single sample instead of examining samples in a wide range of loadings; (iv) recording of vibrational spectra at one single temperature *etc.* Hence, temperature and loading effects have often been overlooked.

Indeed, temperature dependent speciations of distinct dispersed oxometallic species are established for MoO_x, WO_x, ReO_x and VO_x sites supported on TiO_2,[18–20,23,24] whereas the prevalence of particular configurations depending on coverage is also demonstrated.[16,20,23] A holistic approach in the protocol followed for studying the molecular structure of dispersed metal oxide overlayers should include the use of both *in situ* Raman and *in situ* FTIR spectroscopies, ideally complemented by $^{18}O/^{16}O$ isotope exchange.

The present work is concerned with unraveling the molecular structure and termination configuration of the species constituting the $(ReO_x)_n$ phase dispersed on monoclinic ZrO_2. The Re=O terminal stretching vibrational wavenumbers of dispersed ReO_x sites with mono-oxo, di-oxo and tri-oxo termination configuration lie close to each other.[16,20,25,26] Hence, locating the band wavenumbers with sufficient accuracy is not adequate for differentiating between mono-oxo, di-oxo and tri-oxo configurations. To this end, *in situ* Raman and *in situ* FTIR spectroscopies (the latter in the overtone region) are used in the temperature range of 400–80 °C for a wide range of surface coverage (0.71–3.7 Re nm^{-2}) in order to shed light in the issue of heterogeneity (*i.e.* determine the number of species present and their relative presence depending on temperature and coverage). Moreover, by exploiting the vibrational selection rules of Raman and FTIR spectroscopy as well as the vibrational isotope effects, a differentiation between the various termination configurations is proposed.

2. Experimental section

2.1. Synthesis and textural characterization of ReO_x/ZrO_2 catalysts

The preparation of the ReO_x/ZrO_2 materials took place by incipient wet impregnation of monoclinic ZrO_2 (Alfa Aeasar), which was calcined prior to its use at 600 °C (heating rate, 2 °C min^{-1}) for 4 h. Pre-weighed amounts of precursor NH_4ReO_4 (Alfa Aeasar) corresponding to targeted coverages were dissolved in triply distilled water resulting to Re(VII) concentrations in the range of 1.6×10^{-3}–8.2×10^{-3} M at pH = 7.5 that was adjusted by dropwise adding NH_3 or HNO_3 solutions. The solution speciation of oxo-Re(VII) species was examined by Raman spectroscopy (Fig. S1, ESI†) and it was confirmed that all precursor solutions contained Re exclusively in the form of ReO_4^- ions.

For each synthesis, a weighed amount of the pre-calcined support was added in the precursor solution that was equilibrated at 45 °C for 1 h by continuous monitoring and periodic adjustment of the pH (pH = 7.5), and subsequently the solvent was removed by rotary evaporation. The obtained materials were dried for 16 h at 120 °C and were afterwards calcined in a muffle furnace at 450 °C for 3 h under static air. The resulting Re loading (wt% Re) for each sample was determined by icp-analysis and was found -as expected-[20] lower than previewed from the weighed-in amounts of NH_4ReO_4 and ZrO_2 due to partial loss of the volatile rhenium oxide by vaporisation.

The specific surface area of the catalysts was determined by the BET method based on N_2 adsorption–desorption isotherms as described previously.[20] Hence, the actual Re surface density for each sample, n_s (expressed as Re nm^{-2}), could be calculated as

$$n_s = \frac{\left[\frac{g_{Re}}{g_{cat}}/A_{Re}\right] \times 6.023 \times 10^{23}}{\left[S_{BET}/(m^2\ g_{cat}^{-1} \times 10^{18}\ nm^2\ m^{-2})\right]} \qquad (1)$$

where A_{Re} is the atomic mass of Re in amu.

The only crystalline phase contained in the prepared samples was, as determined by powder XRD diffraction, monoclinic ZrO_2. Table 1 compiles the principal characteristics for each catalyst sample, denoted as $uReZrO_2$, where u is the surface density in Re nm^{-2}.

2.2. Raman and FTIR spectroscopy. Protocols of measurements

2.2.1. *In situ* steady state Raman spectra under dehydrated feed conditions.
A homemade optical Raman cell was used for obtaining the *in situ* Raman spectra for the $ReO_x/ZrO_2(m)$ materials at steady state under oxidative dehydrated conditions. A detailed description of the *in situ* Raman cell can be found in previous reports.[27,28] Each sample (130–140 mg), in the form of a pressed wafer made using a hydraulic press at a load of ~25 kN, was mounted on the *in situ* Raman cell sample supporter. The cyan 491.5 nm line of a DPSS laser (Cobolt Calypso) was used as the excitation source. The laser power on the wafer was ~10 mW. The illumination spot on the wafer was ~2 mm^2, adjusted by slightly defocusing the incoming beam by a cylindrical lens, thereby reducing sample irradiance. The scattered radiation was collected at right angle on a horizontal scattering plane and analysed by a Spex 1403 0.85 m double monochromator. The signal was detected by a −20 °C – cooled RCA photomultiplier tube interfaced with a Labspec software.

To ascertain that the calcined $uReZrO_2$ samples do not undergo further gradual ReO_x loss due to ReO_x vaporization, the following procedure was followed for each sample. First, each sample was heated to 400 °C for 1 h in the *in situ* Raman cell under flowing (30 $cm^3\ min^{-1}$) 20% O_2/He gas mixture (He 99.999% and O_2 99.999% form L' Air Liquide). Subsequently,

temperature was lowered to 250 °C under flowing 20% O_2/He gas and the *in situ* Raman spectrum was recorded after 1 h and 45 min on stream. Temperature was then raised to 400 °C and an *in situ* Raman spectrum was obtained under flowing 20% O_2/He gas as reference at 400 °C after 1 h and 45 min on stream. Finally, temperature was lowered again to 250 °C and after 1 h and 45 min exposure to flowing 20% O_2/He gas the *in situ* Raman spectrum at 250 °C was reproduced. Fig. S2 (ESI†) show the pertinent *in situ* Raman spectra obtained at 250 °C for three representative samples (0.71ReZrO₂, 1.3ReZrO₂ and 2.4ReZrO₂), before and after the intermediate exposure of the sample at 400 °C under flowing feed gas for ~3 h and 15 min. It is evident that the spectra are fully reproduced and hence following the initial partial loss of ReO_x due to vaporization during the calcination stage, no further loss of ReO_x had taken place.

Recording of *in situ* Raman spectra under continuous dehydrated feed conditions (30 $cm^3\ min^{-1}$ 20% O_2/He) started at 400 °C after 1 h and 45 min on stream. Temperature was subsequently lowered to 250, 225, 200, 175, 145, 120, 100, 80, 60 and 35 °C using both a sequential and a random order of temperatures, and steady state *in situ* Raman spectra were collected after 1 h and 45 min sample treatment at each temperature to ensure steady state attainment. After recording the *in situ* Raman spectra at a certain temperature, the sample was first heated to 400 °C for 1 h and then cooled to the next temperature. After completing each sequence, the sample under study was heated to 400 °C and the full reinstatement of its structural state was checked and confirmed by reproducing the pertinent *in situ* Raman spectrum at 400 °C. The spectral resolution was set to 7 cm^{-1} by appropriate adjustments of the entrance and exit monochromator vertical slits' apertures. A high signal-to-noise ratio could be achieved by performing slow scans with a 1.2 s photon counting per point at 0.25 cm^{-1} increments. A normalisation procedure of the obtained Raman spectra, previously described in detail,[20,29] was implemented for normalising the spectra and compensate the "path length" effect caused by the coloured samples in the wide 0.71–3.7 Re nm^{-2} coverage range studied. Very briefly, first the background of each spectrum was zeroed by subtracting a rectangle, thereby zeroing the counts of the high wavenumber tail of the spectrum and subsequently the whole spectrum was divided by the area under the spectrum trace in the 270–1100 cm^{-1} wavenumber range that features the main Raman bands of structural relevance.

2.2.2. *In situ* steady state FTIR spectra under dehydrated feed conditions.
The *in situ* FTIR study was undertaken using an *in situ* DRIFT cell (Spectra Tech) on a FTIR Nicolet 6700 spectrometer equipped with a KBr beam splitter and an MCTB detector. The procedure followed was identical to the one used for the *in situ* Raman study. Each catalyst sample was first exposed for 1 h at 400 °C under dry flowing (30 $cm^3\ min^{-1}$) 20% O_2/He and the *in situ* FTIR spectrum at 400 °C was recorded. 64 scans were averaged for each spectrum at a resolution set to 4 cm^{-1}. Subsequently, sequential *in situ* steady state FTIR spectra were recorded at temperatures of 250,

Table 1 $ReO_x/ZrO_2(m)$ catalysts' characteristics (initial Re(VII) concentration of precursor solution, wt% Re loading, BET surface area and Re surface density). Precursor solution pH: 7.5. Calcination: 450 °C, 3 h[a]

Catalysts	$C_{Re(VII)}$ (M)	Loading (wt% Re)[b]	S_{BET} ($m^2\ g^{-1}$)	n_s (Re nm^{-2})
0.71ReZrO₂	1.6×10^{-3}	1.09	50	0.71
1.3ReZrO₂	3.3×10^{-3}	2.08	52	1.3
1.5ReZrO₂	4.1×10^{-3}	2.43	52	1.5
1.9ReZrO₂	5.0×10^{-3}	3.08	53	1.9
2.4ReZrO₂	5.8×10^{-3}	3.64	49	2.4
3.7ReZrO₂	8.2×10^{-3}	5.33	46	3.7

[a] Support $ZrO_2(m)$ pre-calcined at 600 °C for 4 h; S_{BET,ZrO_2}: 50 $m^2\ g^{-1}$.
[b] As per icp analysis.

175, 120 and 400 °C (following 1 h and 45 min exposure under flowing 20% O_2/He at each temperature). The reinstatement of the catalyst molecular structure at 400 °C was verified by reproducing the pertinent spectrum corresponding to each sample. The overtone Re=O stretching spectral range is studied due to strong absorption in the corresponding fundamental stretching region. Reference *in situ* FTIR spectra under flowing 20% O_2/He were recorded at each temperature also for the pure support ZrO_2 and were subtracted from the *in situ* FTIR spectra obtained for the samples studied. Hence, difference spectra pertaining to the dispersed $(ReO_x)_n$ phase are reported below.

2.2.3. *In situ* Raman/^{18}O isotope exchange study. The procedure for setting up the protocol for undertaking the *in situ* Raman–^{18}O/^{16}O exchange experiments at 400 °C was established by simulating the pertinent reduction/oxidation cycles using a 4.5% H_2/He mixture (H_2 99.999% from L' Air Liquide) as the reductant and a 2% ^{16}O$_2$/He gas mixture as the oxidant, as described previously.[30,31] It was found that under the specified conditions, a 20 min duration was necessary to attain a sufficient reduction, whilst 10 min were required for an adequate reoxidation by a 2% ^{16}O$_2$-containing gas. Accordingly, each ^{18}O/^{16}O isotope exchange redox cycle was made up of a 20 min reduction step under flowing (30 cm^3 min^{-1}) 4.5% H_2/He and a 10 min oxidation step under flowing (10 cm^3 min^{-1}) 2% ^{18}O$_2$/He (Linde, certified mixture). Up to 25 redox ^{18}O/^{16}O isotope exchange cycles were undertaken for each studied catalyst sample and *in situ* Raman spectra were periodically recorded at 400 °C after a specified number of ^{18}O/^{16}O isotope exchange cycles.

3. Results and discussion

The ReO_x deposition on $ZrO_2(m)$ takes place inside the precursor suspension that contain Re exclusively in the form of ReO_4^- moieties (see Fig. S1†) and proceeds *via* Zr–O–Re(–O)$_3$ and/or (Zr–O)$_2$–Re(–O)$_3$ anchoring (where in the latter case one of the Zr–O–Re anchors involves also a ZrO_2 lattice O). Drying and calcination follows the well-established mechanism of gradual titration of surface hydroxyls by means of successive esterification-like steps and concomitant condensation of water molecules that remain retained by means of H-bonding to the surface layer.[18–20,23,24,32–38] Hence, after the initial anchoring, bipedal and gradually multipedal ReO_x units are formed at the expense of terminal Re–O sites. Therefore, as established for several supported MO_x transition metal oxides (M = V, Mo, W, Re) for surface coverages below the respective monolayer limit, formation of distinct species takes place in the course of the calcination resulting in heterogeneity of the dispersed MO_x phase.[16,18–21,23,24,38] Additionally, when coverage exceeds a certain limit, which is characteristic for each system, M–O–M associations take place resulting in $(MO_x)_n$ domain growth.[22]

3.1. *In situ* molecular vibrational (Raman, FTIR) spectra of $ReO_x/ZrO_2(m)$ catalysts. Coverage and temperature effects

3.1.1. Effect of Re coverage. Fig. 1 shows the effect of Re coverage (in the range of 0.71–3.7 Re nm^{-2}) on the *in situ* Raman spectra obtained for all $ReO_x/ZrO_2(m)$ catalysts studied at constant temperature of 400 °C (Fig. 1A), 250 °C (Fig. 1B) and 175 °C (Fig. 1C). Normalised Raman spectra[20,29] are
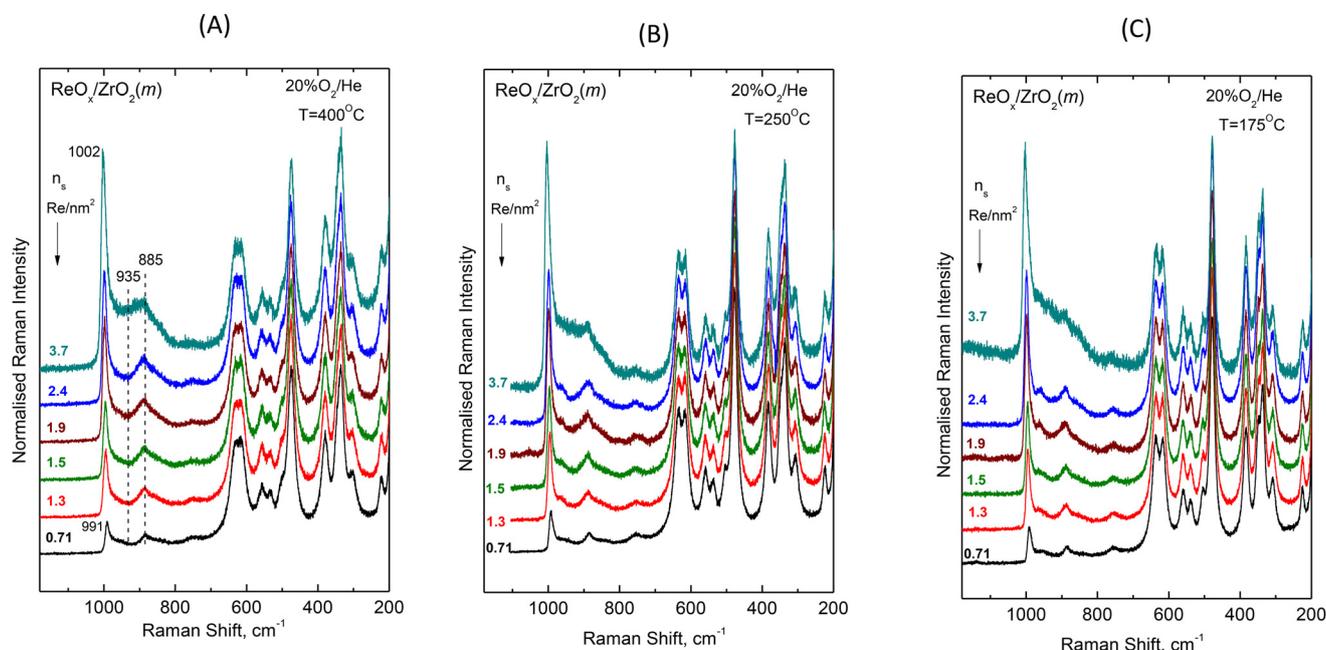
Fig. 1 Effect of coverage on the *in situ* Raman spectra obtained for ReO_x/ZrO_2 catalysts under flowing 20% O_2/He at temperatures of: (A) 400 °C; (B) 250 °C; and (C) 175 °C at coverages in the 0.71–3.7 Re nm^{-2} range as indicated by each spectrum. The full spectral range of 200–1100 cm^{-1} is shown. Recording parameters: laser wavelength, λ_0 = 491.5 nm; laser power, w = 10 mW; time constant, τ = 0.3 s; spectral slit width, ssw = 7 cm^{-1}.

shown in the full spectral region including the contribution of bands due to monoclinic ZrO_2, which are confined up to *ca.* 750 cm^{-1}.[39] Fig. 2(A–C) shows the corresponding evolution of the *in situ* normalized Raman spectra with increasing Re coverage, obtained with higher S/N ratio and focused in the wavenumber range pertaining to stretching Re=O and Re–O– modes. First observations of spectral effects in Fig. 1 and 2 include: (i) the convoluted band envelope due to terminal Re=O stretching is asymmetric with evidence of several overlapping bands in the Re=O stretching region that are known to occur at wavenumbers typically higher than 940 cm^{-1};[16,25,26] (ii) the peak maximum of the Re=O band envelope undergoes a pronounced blue shift with increasing coverage, *e.g.* from 991 cm^{-1} for 0.71 Re nm^{-2} to 1002 cm^{-1} for 3.7 Re nm^{-2} at 400 °C; (iii) with increasing coverage, a broad band at ~885 cm^{-1} progressively loses intensity relative to the *ca.* 990–1000 cm^{-1} Re=O stretching band envelope; and (iv) a broad, however obscured, band at ~935 cm^{-1} emerges and progressively gains intensity with increasing coverage, becoming discernible for $n_S \geq 1.3$ Re nm^{-2}. The wavenumber location and broad nature of the latter two bands (*i.e.* at ~885 and ~935 cm^{-1}) are suggestive of Re–O– provenance (*i.e.* Re–O–Re, O–Re–O and Re–O–Zr).

With increasing coverage, the ReO_x domains are expected to grow by means of Re–O–Re associations at the expense of Re–O–Zr anchors. Hence, with increasing coverage the Re–O–Re/Re=O ratio is expected to increase and the Re–O–Zr/Re=O ratio is expected to decrease. In view of the above, the ~885 cm^{-1} band that loses intensity relative to the Re=O envelope with increasing coverage is assigned to Re–O–Zr

modes and the ~935 cm^{-1} band that gains intensity relative to the Re=O envelope with increasing coverage is assigned to Re–O–Re modes. Additional evidence strengthening the assignment of the ~885 cm^{-1} band to Re–O–Zr modes will be presented and discussed below, in the context of the temperature dependence of *in situ* Raman spectra.

A first discussion of the blue-shifting tendency observed with increasing coverage for the band envelope ascribed to terminal Re=O stretching should include a consideration of factors affecting the wavenumber of the terminal Re=O stretching. Such factors may include *inter alia*: (a) the termination configuration (*i.e.* mono-oxo, di-oxo *etc.*); (b) the Re coordination number; (c) vibrational coupling (particularly in case of occurrence of Re–O–Re associations); and (d) variations in basicity of support dative O atoms. In the initial steps of ReO_x deposition, the most basic surface hydroxyls are titrated first, hence with increasing coverage hydroxyls with lower basicity come gradually into play and by that means – in a cascade effect – the terminal Re=O stretching becomes gradually stronger thereby partly justifying the corresponding blue shift with increasing coverage (*e.g.*, from 991 to 1002 cm^{-1} at 400 °C, Fig. 2(A)).

Fig. 3 shows the evolution of the *in situ* FTIR spectra obtained at constant temperature of 400 °C (Fig. 3A), 250 °C (Fig. 3B) and 175 °C (Fig. 3C) for ReO_x/ZrO_2 catalysts with coverages of 0.71, 1.3 and 2.4 Re nm^{-2} under dehydrating feed conditions of flowing (30 cm^3 min^{-1}) 20% O_2/He gas. The spectra are obtained in the overtone region, hence the wavenumber span of the terminal stretching region is approximately doubled. Likewise, the mutual distance between the
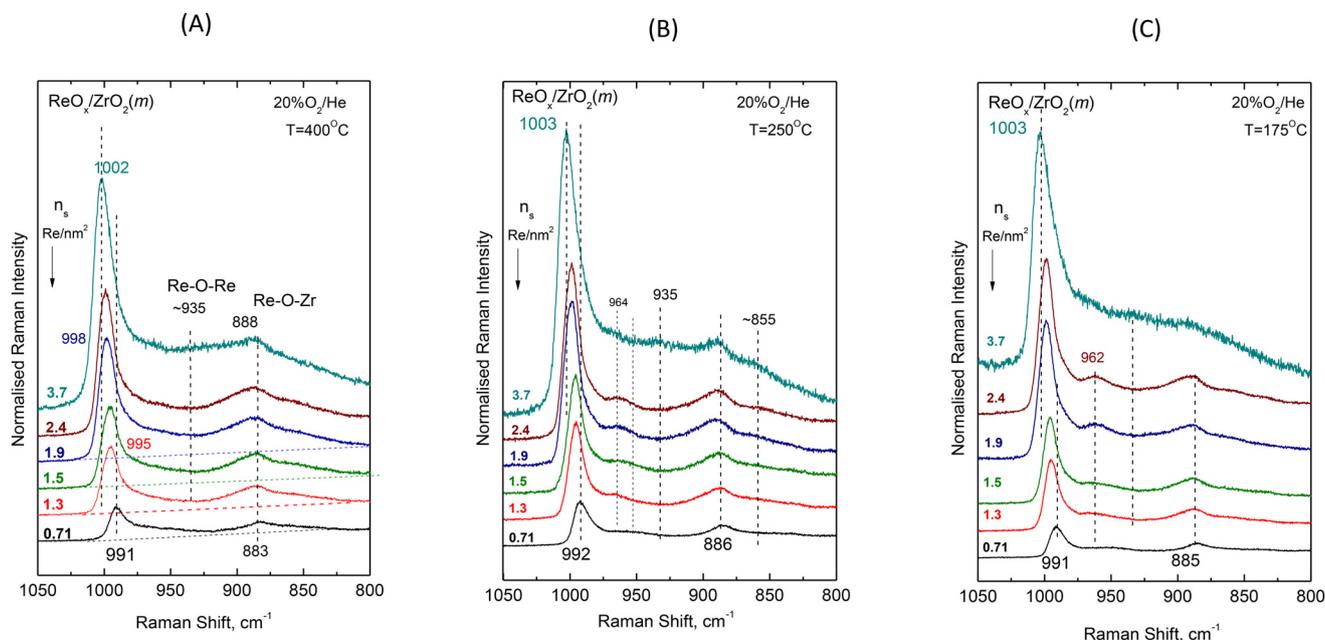
Fig. 2 Effect of coverage on the *in situ* Raman spectra obtained for ReO_x/ZrO_2 catalysts under flowing 20% O_2/He at temperatures of: (A) 400 °C; (B) 250 °C; and (C) 175 °C at coverages in the 0.71–3.7 Re nm^{-2} range as indicated by each spectrum. The Re–O stretching region of 800–1050 cm^{-1} is shown. Recording parameters: laser wavelength, $\lambda_0 = 491.5$ nm; laser power, $w = 10$ mW; time constant, $\tau = 1.2$ s; spectral slit width, ssw = 7 cm^{-1}.
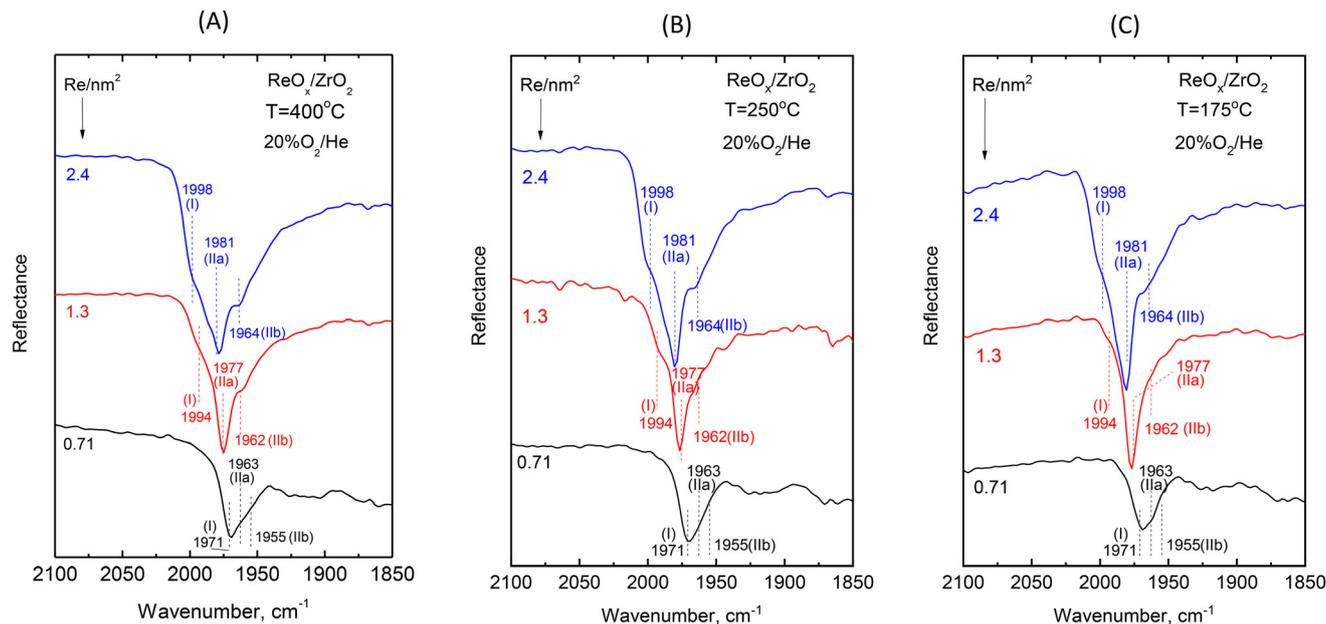
Fig. 3 Effect of coverage on the *in situ* FTIR spectra obtained for ReO$_x$/ZrO$_2$ catalysts under flowing 20% O$_2$/He at temperatures of: (A) 400 °C; (B) 250 °C; and (C) 175 °C at coverages of 0.71, 1.3 and 2.4 Re nm^{-2} as indicated by each spectrum. The corresponding spectra obtained for ZrO$_2$ have been subtracted. The dotted lines mark the band wavenumbers for the symmetric stretching modes of Species-I, Species-IIa and Species-IIb deduced by exploiting the respective temperature dependent features portrayed in Fig. 4(B), 5(B) and 6(B). Resolution, 4 cm^{-1}.

infrared bands corresponding to the counterpart Raman components comprising the terminal stretching band envelope observed in the Raman spectra (Fig. 2) is also approximately doubled resulting in clearly distinct bands in Fig. 3, thereby ascertaining the multiple character ascribed to the observed "broad" terminal stretching Raman band envelopes (Fig. 2) and excluding the possibility for certain bands as being simply of broad nature.

3.1.2. Effect of temperature. Fig. 4–6 show the effect of temperature on the *in situ* Raman and *in situ* FTIR spectra obtained for ReO$_x$/ZrO$_2$ samples under dehydrated feed conditions (flowing 20% O$_2$/He gas mixture) in the temperature range of 400–120 °C at constant surface coverages of 0.71 Re nm^{-2} (Fig. 4), 1.3 Re nm^{-2} (Fig. 5) and 2.4 Re nm^{-2} (Fig. 6). The spectral regions of Re=O and Re–O– stretching modes are portrayed. Panels 4(A), 5(A) and 6(A) pertain to *in situ* Raman spectra, whilst panels 4(B), 5(B) and 6(B) pertain to the counterpart *in situ* FTIR spectra. All spectra are recorded at a sequential order of decreasing temperatures. Notably, as mentioned also in the Experimental section, reheating the samples to 400 °C under flowing 20%O$_2$/He results in full reinstatement of the corresponding spectrum in each case. Additionally, Fig. S3(A–F)† shows the temperature dependence of the *in situ* Raman spectra obtained for all six samples studied in the full temperature range of 400–35 °C. We shall, however, confine the discussion mainly to Fig. 4–6 that are adequate for inferring the number of species present and their respective termination configurations. The extent of the temperature-dependent changes observed vary with surface coverage, as discussed below.

Low coverage ReO$_x$/ZrO$_2$ with 0.71 Re nm^{-2}. The rhenium–oxygen terminal stretching modes are known to occur in the 940–1010 cm^{-1} region depending on the termination configuration and on the identity of the surrounding ligands.[16,20,25,26] Fig. 4(A) shows a pertinent multi-component band envelope exhibiting a strong feature at 995–975 cm^{-1} (presumably due to symmetric terminal stretching modes)[20,25,26] and a 975–940 cm^{-1} tail, probably due to antisymmetric modes (of *e.g.* di-oxo sites) that are known to be weaker and to occur at 10–40 cm^{-1} lower than their respective symmetric counterpart modes.[20,25,26,28] The temperature-dependent variations of the relative band intensities in Fig. 4 (A) imply a corresponding temperature-dependent prevalence of distinct dispersed ReO$_x$ species, thereby corroborating the proposal for the heterogeneity of the dispersed rhenia phase. The counterpart *in situ* FTIR spectra displayed in Fig. 4(B) show a better separation amongst the respective component bands due to the approximate doubling of their mutual distances in the overtone region. Hence, the main FTIR band envelope due to Re–O terminal symmetric stretching has three clearly discerned components at 1971, 1963 and 1955 cm^{-1} plus two weaker broad features at ~1920 and ~1870 cm^{-1}. The temperature dependent features of the relative intensities observed for the 1971, 1963 and 1955 cm^{-1} bands in Fig. 4(B) show that their prevalence is due to three distinct ReO$_x$ species. Hence, the asymmetric 975–995 cm^{-1} Raman band envelope in Fig. 4(A) is reasonably thought to consist of three component bands.

In order to corroborate the evidence supporting the above proposal we performed a peak analysis in the terminal stretch-

(A)

(B)
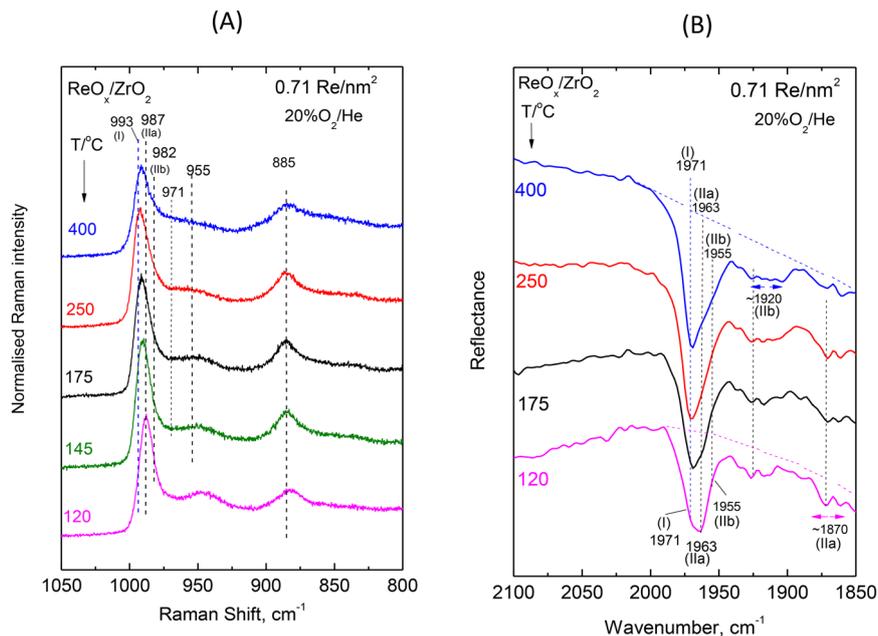
Fig. 4 ReO_x/ZrO_2 with surface density of 0.71 Re nm^{-2}: (A) sequential (430 → 250 → 175 → 145 → 120 °C) *in situ* Raman spectra obtained under flowing 20%O$_2$/He at temperatures as indicated by each spectrum. Spectral recording parameters: see Fig. 2 caption. (B) Sequential (430 → 250 → 175 → 120 °C) *in situ* FTIR spectra obtained under flowing 20% O$_2$/He at temperatures as indicated by each spectrum. The corresponding spectra obtained for ZrO$_2$ have been subtracted. Resolution, 4 cm^{-1}.

(A)

(B)
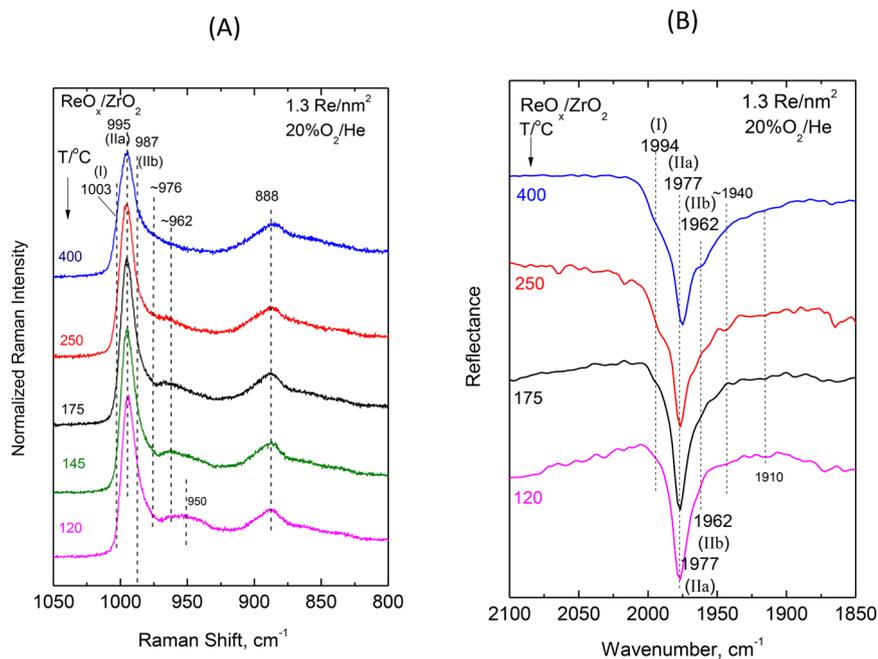
Fig. 5 ReO_x/ZrO_2 with surface density of 1.3 Re nm^{-2}: (A) sequential (430 → 250 → 175 → 145 → 120 °C) *in situ* Raman spectra obtained under flowing 20%O$_2$/He at temperatures as indicated by each spectrum. Spectral recording parameters: see Fig. 2 caption. (B) Sequential (430 → 250 → 175 → 120 °C) *in situ* FTIR spectra obtained under flowing 20% O$_2$/He at temperatures as indicated by each spectrum. The corresponding spectra obtained for ZrO$_2$ have been subtracted. Resolution, 4 cm^{-1}.

ing region of the *in situ* Raman spectra shown in Fig. 4(A) and the results are shown in Fig. 7(A). The criteria for the peak analysis of the Re($=$O)$_2$ terminal stretching region invoke:

(1) The occurrence of five bands due to three Species, as evidenced from the combined observations of the *in situ* Raman and FTIR spectra as follows: (i) one band at the highest wave-
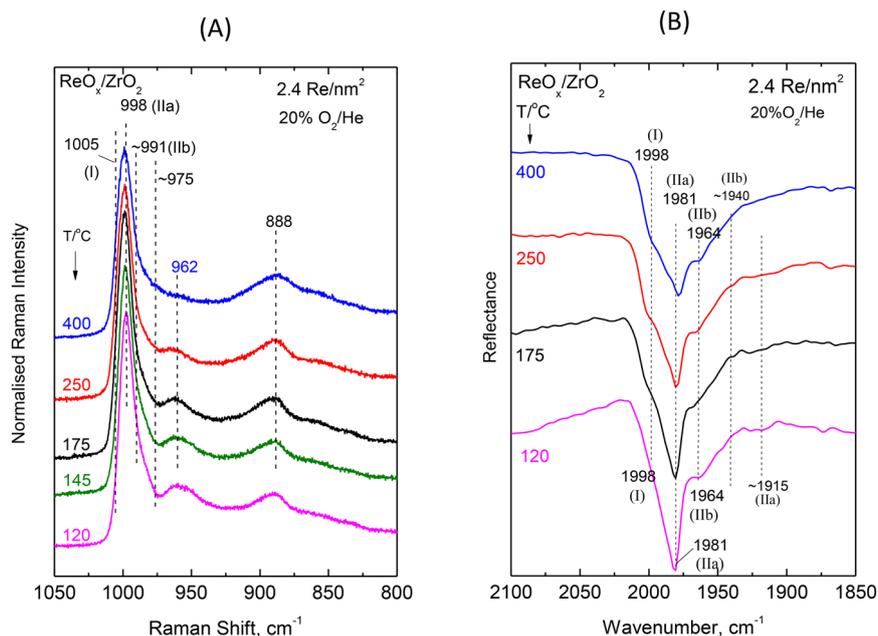
Fig. 6 ReO$_x$/ZrO$_2$ with surface density of 2.4 Re nm^{-2}: (A) Sequential (430 → 250 → 175 → 145 → 120 °C) *in situ* Raman spectra obtained under flowing 20%O$_2$/He at temperatures as indicated by each spectrum. Spectral recording parameters: see Fig. 2 caption. (B) Sequential (430 → 250 → 175 → 120 °C) *in situ* FTIR spectra obtained under flowing 20% O$_2$/He at temperatures as indicated by each spectrum. The corresponding spectra obtained for ZrO$_2$ have been subtracted. Resolution, 4 cm^{-1}.
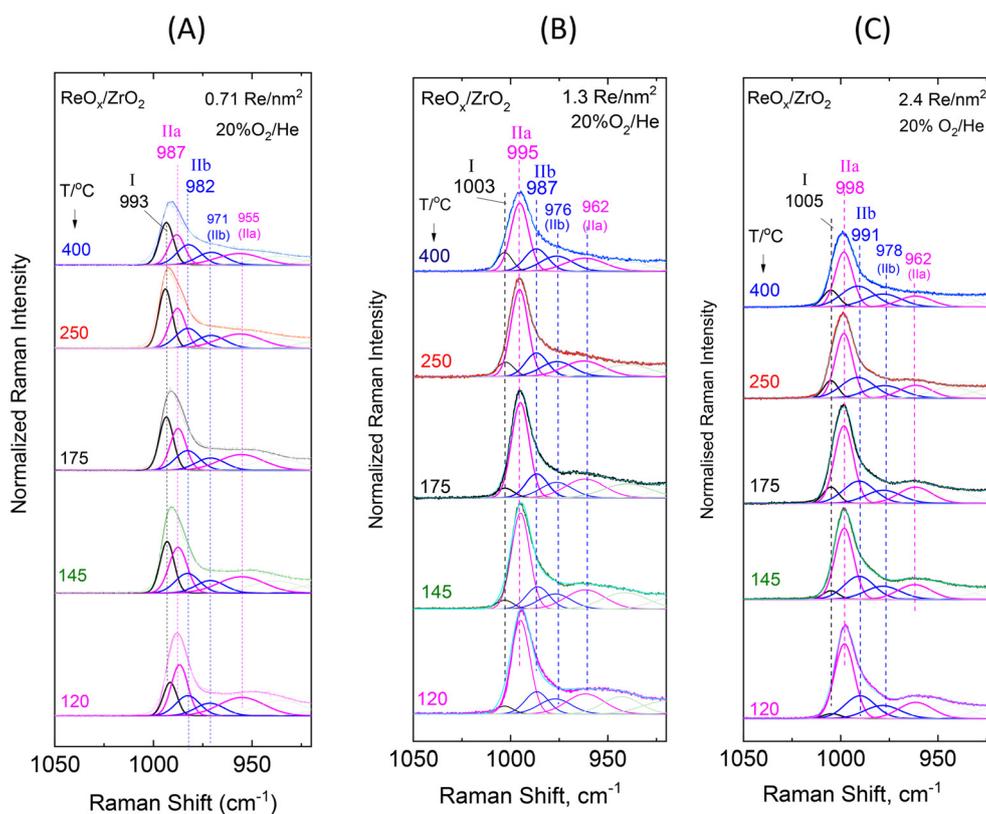
Fig. 7 Sequential (430 → 250 → 175 → 145 → 120 °C) *in situ* Raman spectra obtained under flowing 20% O$_2$/He at temperatures as indicated by each spectrum for ReO$_x$/ZrO$_2$ with surface densities of: (A) 0.71 Re nm^{-2}; (B) 1.3 Re nm^{-2}; and (C) 2.4 Re nm^{-2}. Peak analysis is shown. The corresponding spectra obtained for ZrO$_2$ have been subtracted. Spectral recording parameters: see Fig. 2 caption.

number due to the terminal Re=O stretching mode of Species-I; (ii) two bands due to the ν_s/ν_{as} pair due to Species-IIa with $\nu_s - \nu_{as} \approx 10\text{–}40$ cm^{-1}; and (iii) two bands due to the ν_s/ν_{as} pair due to Species-IIb with $\nu_s - \nu_{as} \approx 10\text{–}40$ cm^{-1}

(2) Fixed band widths and positions (with allowance for the measurement precision, *i.e.* ±1 cm^{-1}) for each studied sample with surface densities of 0.71, 1.3 and 2.4 Re nm^{-2}

(3) Fixed relative $I_{\nu_s}/I_{\nu_{as}}$ intensities for each dioxo species (IIa, IIb), and

(4) Allowance for broader ν_{as} bands compared to their respective ν_s counterparts.

The results of the peak analysis show that three peaks are found in the 975–1000 cm^{-1} symmetric terminal stretching region, at 993, 987 and 982 cm^{-1}, whilst the low wavenumber tail is fitted with two further broader bands at 971 and 955 cm^{-1}, presumably due to antisymmetric terminal stretching modes. Pairing of bands (*i.e.* assignment of two bands to the same species) can be justified when their mutual relative intensities are maintained in the full temperature range. In view of this principle, the 993 cm^{-1} band is solely assigned to Species-I, the 987/955 cm^{-1} pair is assigned to Species-IIa and the 982/971 cm^{-1} pair to Species-IIb.

The temperature-dependent behavior of the 993 (I), 987 (IIa) and 982 (IIb) cm^{-1} bands (Fig. 7) shows that with increasing temperature the relative intensity of the 993 cm^{-1} band due to Species-I is increased at the expense of the 987 cm^{-1} band (Species-IIa), whilst the 982 cm^{-1} component (Species-IIb) does not undergo discerned relative intensity changes in the 120–400 °C range. As shown previously for ReO$_x$/TiO$_2$ [20] and ReO$_x$/CeO$_2$ [21] catalysts a O=ReO$_n$ species with mono-oxo termination configuration is favored at low coverage and high temperature, hence Species-I with a single Re=O stretching mode at the highest wavenumber of 993 cm^{-1} among all bands has a mono-oxo O=ReO$_n$ configuration. Species IIa and IIb, both possess terminal stretching band pairs at 987/955 cm^{-1} and 982/971 cm^{-1} conforming to the ν_s/ν_{as} (*i.e.* symmetric/antisymmetric) expected pair for sites that take on a dioxo termination configuration that is expected to give rise to a symmetric stretching mode, ν_s, with higher intensity compared to an antisymmetric stretching mode, ν_{as}, at wavenumbers conforming to the $\nu_s - \nu_{as} = {\sim}10\text{–}40$ cm^{-1} rule.[25] The above observations in the temperature range of 120–400 °C are interpreted to indicate the following temperature-dependent reversible transformation

$$\underset{\text{Species–I}}{\text{O=Re}(-\text{O–Zr})_m} + \text{HOH} + (\text{Zr–O–})$$

$$\underset{\text{T-raising}}{\overset{\text{T-lowering}}{\rightleftharpoons}} \underset{\text{Species–IIa}}{(\text{O=})_2\text{Re}(-\text{O–Zr})_{m-1}} + \text{Zr–OH} + \text{Zr–OH} \quad \text{(A)}$$
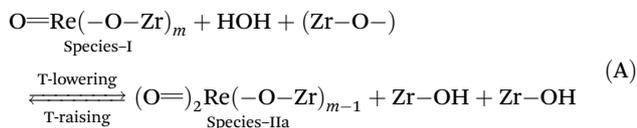
A molecular-level mechanism for the above reaction scheme (A) portraying plausible molecular models for Species–I and Species–IIa is shown in Fig. 8. Water molecules retained at the surface layer of oxide carriers by means of H-bonding have previously also been shown to mediate temperature-dependent transformations among distinct MO$_x$ sites in ReO$_x$/

O=Re(–O–Zr)$_m$
Species - I

(O=)$_2$Re(–O–Zr)$_{m-1}$
Species - IIa
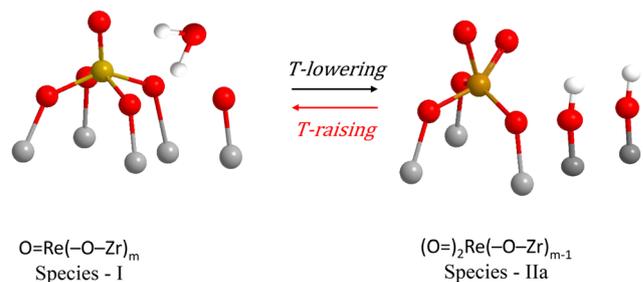
Fig. 8 Molecular-level mechanism accounting for the reversible temperature-dependent Species-I ↔ Species-IIa transformation mediated by water molecules retained at the surface layer and surface hydroxyls. For simplicity, mononuclear representations are shown. The number of anchoring bonds and the resulting coordination number, CN$_{Re}$ = 5 are reasonable in view of the oxidation state VII for Re. Gold spheres, Re; red spheres, O; grey spheres, Zr. H atoms (white spheres) are included to account for hydroxylation (see text).

TiO$_2$, WO$_x$/TiO$_2$, MoO$_x$/TiO$_2$ and VO$_x$/TiO$_2$ catalysts.[18–20,23,24] Such water molecules retained at the support oxide surface layers by H-bonding are formed during the titration of surface hydroxyls that takes place by the precursor oxometallic species during the deposition steps.[32–37]

Notably, the reaction scheme shown in Fig. 8 implies that with increasing temperature a gradual increase of Re–O–Zr anchors will take place thereby resulting in an increase of the Re–O–Zr/Re=O ratio. Indeed, as seen in Fig. 4A, a relative strengthening of the ${\sim}885$ cm^{-1} band is observed with increasing temperature, thereby corroborating the initial assignment of the ${\sim}885$ cm^{-1} band (see section 3.1.1 pertaining to the effect of coverage) to Re–O–Zr anchors.

The temperature-dependent features of the *in situ* FTIR spectra obtained for the low coverage 0.71 Re nm^{-2} sample are in full conformity with the above scenario of temperature-dependent interplay involving the mono-oxo Species-I and dioxo Species-IIa as well as the relative stability of di-oxo Species-IIb in the temperature range of 120–400 °C. On grounds of anharmonicity, which allows the observation of first overtones, the 993, 987 and 982 cm^{-1} stretching fundamentals due to Species-I (mono-oxo), Species-IIa (dioxo) and Species-IIb (dioxo) are expected to give overtones at wavenumbers slightly below the respective doubled fundamentals,[25,40] *i.e.* the ${\sim}1971$, ${\sim}1963$ and ${\sim}1955$ cm^{-1} observed wavenumbers conform to the above rule. With increasing temperature, the 1963 cm^{-1} band due to Species-IIa diminishes and the 1971 cm^{-1} Species-I band prevails, whilst the 1955 cm^{-1} Species-IIb band remains unaffected and is better discerned at 400 °C where the 1963 cm^{-1} Species-IIa band has diminished. The ${\sim}1920$ and ${\sim}1870$ cm^{-1} broad bands are assigned to the first overtones of the antisymmetric 971 and 955 cm^{-1}, ν_{as}, modes of Species-IIb and Species-IIa, respectively.

Intermediate and high coverage ReO$_x$/ZrO$_2$ with 1.3 and 2.4 Re nm^{-2}. Decoding of the temperature-dependent features of the *in situ* Raman and *in situ* FTIR spectra obtained for the ReO$_x$/ZrO$_2$ catalysts with 1.3 and 2.4 Re nm^{-2} shown in Fig. 5(A, B) and 6(A, B) becomes straight-forward in view of the findings

discussed for the temperature dependent spectral features for the low coverage 0.71ReZrO_2 sample (*vide ante*) and the general coverage effect trends presented in section 3.1.1.

The splitting pattern of the FTIR overtones in the symmetric stretching overtone 1960–2000 cm^{-1} region of the spectra shown in Fig. 5(B) and 6(B) reveals in each case the occurrence of three distinct bands due to Species-I, Species-IIa and Species-IIb. As discussed in section 3.1.1 (Fig. 3) all stretching band wavenumbers exhibit a gradual blue shift with increasing coverage in the range 0.71–3.7 Re nm^{-2} studied. Moreover, it is evident that whereas for a low coverage of 0.71 Re nm^{-2} the mono-oxo Species-I prevails at *e.g.* 400 °C, this is no longer the case for higher coverages of 1.3 and 2.4 Re nm^{-2} where, as best seen in the *in situ* FTIR spectra shown in Fig. 5B and 6B, Species-I is a minority species at 400 °C.

The interpretation and the pertinent discussions are facilitated by performing a peak analysis in the terminal stretching region of the *in situ* Raman spectra shown in Fig. 5A and 6A, obtained for 1.3ReZrO_2 and 2.4ReZrO_2, and the results of the peak analysis are shown in Fig. 7B and C. The band wavenumbers assigned to the different species for 1.3ReZrO_2 are at 1003 cm^{-1} (Species-I, Re=O, mono-oxo), 995/962 cm^{-1} (ν_s/ν_{as}, Species-IIa, di-oxo) and 987/976 cm^{-1} (ν_s/ν_{as}, Species-IIb, di-oxo). The respective wavenumbers for 2.4ReZrO_2 are at 1005 cm^{-1} (Species-I, Re=O, mono-oxo), 998/962 cm^{-1} (ν_s/ν_{as}, Species-IIa, di-oxo) and 991/978 cm^{-1} (ν_s/ν_{as}, Species-IIb, di-oxo). Table 2 compiles the band wavenumbers and assignments for the various species.

As seen in Fig. 7B and C, with increasing temperature band (I) due to Species-I (mono-oxo) gains intensity at the expense of the Species-IIa ν_s mode for both 1.3ReZrO_2 and 2.4ReZrO_2. Contrary, however, to the case of the low coverage 0.71ReZrO_2 (Fig. 8A), Species-IIa remains clearly predominant up to 400 °C. Reasonably, the reason lowering the progress of reaction scheme (A) to the left is the increased coverage with its consequent shortage of surface hydroxyls adjacent to Species-IIa caused by their extensive titration during the deposition process.

3.2. *In situ* Raman spectra and $^{18}\text{O}/^{16}\text{O}$ isotopic substitution. Vibrational isotope effects

Complementing *in situ* Raman spectroscopy with $^{18}\text{O}/^{16}\text{O}$ isotopic labelling sheds additional light into the issue of termin-

ation configuration in supported transition metal oxide catalysts.[14,28,41] The vibrational isotope effects, *i.e.* the isotopic splitting pattern of terminal stretching bands and the isotopic shift allow for valid discussions on band assignments to $(\text{M}=^{18}\text{O})_n$ modes (n = 1, 2, 3) and on the issue of discrimination between *e.g.* mono-oxo, di-oxo and tri-oxo configurations.[14,41]

The theory of vibrational isotope effects based on the harmonic oscillator approximation, *i.e.* based on a strictly quadratic potential function, results in justified theoretical predictions for the fundamental stretching $\nu(\text{Re}=^{18}\text{O})_n$ (n = 1, 2) modes' wavenumbers of $^{18}\text{O}/^{16}\text{O}$-substituted terminal $\text{Re}=^{18}\text{O}$ and/or $^{18}\text{O}=\text{Re}=^{18}\text{O}$ sites.[40,42] As a paradigm, the diatomic harmonic approximation for a M=O (M: transition metal) terminal site results in the following formula for the isotopic ratio

Isotopic ratio:

$$\frac{\nu_{\text{M}=^{16}\text{O}}}{\nu_{\text{M}=^{18}\text{O}}} = \sqrt{\frac{\dfrac{1}{m_{\text{M}}} + \dfrac{1}{m(^{16}\text{O})}}{\dfrac{1}{m_{\text{M}}} + \dfrac{1}{m(^{18}\text{O})}}} \tag{2}$$

Indicative values for the isotopic ratio for several M=O terminations have been reported.[14] For the Re=O diatomic harmonic oscillator, the isotopic ratio equals 1.0555. The theory and pertinent equations for triatomic $\text{M}(=\text{O})_2$ "molecules" become more involved and elaborate,[42] however leading to an approximately equal isotopic ratio for the symmetric stretching terminal mode. In accordance, DFT calculations for the effect of $^{18}\text{O}/^{16}\text{O}$ substitution on the symmetric stretching wavenumber for the di-oxo $(\text{O}=)_2\text{Mo}(-\text{O}-\text{Si})_2$ structure result in an isotopic ratio of 1.0507,[43] effectively identical to the 1.0513 isotopic ratio calculated for a diatomic mono-oxo Mo=O configuration based on eq. (2). Hence, whereas calculations for theoretically predicted wavenumbers for $\nu(\text{Re}=^{18}\text{O})_n$ modes can be used for verifying the validity of experimentally observed isotopic shifts, such calculations are not adequate for discriminating between *e.g.* mono-oxo and di-oxo termination configurations. Additionally, experimental results pertaining to well-documented di-oxo $\text{Re}(=\text{O})_2$ terminations on TiO_2 and CeO_2 have shown that the use of the isotopic ratio to calculate the wavenumber of the $^{18}\text{O}/^{16}\text{O}$ substituted site (*e.g.* $\text{Re}=^{18}\text{O}$ or $\text{Re}(=^{18}\text{O})_2$) cannot be used for

Table 2 Observed band wavenumbers for Raman fundamentals and IR first overtones for Re−O stretching modes for Species-I, Species-IIa and Species-IIb and tentative assignments

Re nm^{-2}	Species-I, mono-oxo		Species-IIa, di-oxo				Species-IIb, di-oxo				O−Re−O	Re−O−Zr
	O=Re$(-\text{O}-\text{Zr})_n$		$(\text{O}=)_2\text{Re}(-\text{O}-\text{Zr})_n$				$(\text{O}=)_2\text{Re}(-\text{O}-\text{Zr})_n$					
	$\nu_{1\leftarrow0,R}$	$\nu_{2\leftarrow0,IR}$	$\nu_{s,1\leftarrow0,R}$	$\nu_{as,1\leftarrow0,R}$	$\nu_{s,2\leftarrow0,IR}$	$\nu_{as,2\leftarrow0,IR}$	$\nu_{s,1\leftarrow0,R}$	$\nu_{as,1\leftarrow0,R}$	$\nu_{s,2\leftarrow0,IR}$	$\nu_{as,2\leftarrow0,IR}$		
0.71	993	1971	987	955	1963	~1870	982	971	1955	~1920		885
1.3	1003	1994	995	962	1977	~1910	987	976	1962	~1940	935–940	890
2.4	1005	1998	998	962	1981	~1915	991	978	1964	~1940	935–940	890

differentiating between mono-oxo and di-oxo termination configurations.[20,21]

Fig. 9(A–C) shows the evolution of the *in situ* Raman spectra obtained at 400 °C under flowing (10 cm³ min⁻¹) 2% $^{18}O_2$/He upon successive reduction/oxidation cycles using flowing 5% H_2/He and 2% $^{18}O_2$/He (see Experimental section) for samples with coverage of 0.71 Re nm⁻² (Fig. 9A), 1.3 Re nm⁻² (Fig. 9B) and 2.4 Re nm⁻² (Fig. 9C). The number of redox $^{18}O/^{16}O$ substitution cycles is indicated by each spectrum. The gradual progress of the $^{18}O/^{16}O$ substitution and the consequent evolution of the *in situ* Raman spectra corroborate the aforementioned interpretations and partial conclusions for the occurrence of the three main structural units, namely mono-oxo Species-I, di-oxo Species-IIa and di-oxo Species IIb. Moreover, the observed effects are adequate for further discussions on the reducibility and the relative ease of $^{18}O/^{16}O$ substitution for each individual species.

At 400 °C the ReO_x phase dispersed on the low coverage 0.71ReZrO₂ sample consists of Species-I (mono-oxo, prevalent species), Species-IIa (di-oxo, in significant amount) and Species-IIb (di-oxo, minority species). The following observations are made in Fig. 9A:

(i) After 21 $^{18}O/^{16}O$ substitution redox cycles the band envelope of the convoluted $(Re{=}^{16}O)_n$ modes at ~991 cm⁻¹ exhibits a discerned shoulder at ~982 cm⁻¹. Such a band is assigned to partially $^{18}O/^{16}O$ substituted di-oxo sites ($^{18}O{=}Re{=}^{16}O$).[16,20,21] Theoretical calculations for the wavenumber of a partially substituted di-oxo $^{18}O{=}Mo{=}^{16}O$ site justify further such an assignment.[43]

(ii) During the initial steps of the $^{18}O/^{16}O$ substitution, *i.e.* after 1, 5 and 8 cycles, the band emerging due to the isotopic shift (eventually at ~940 cm⁻¹ after 21 cycles) exhibits a low wavenumber shoulder at ~934 cm⁻¹ indicating a relative ease for the $^{18}O/^{16}O$ substitution of the di-oxo terminal sites of the minority Species-IIb.

(iii) A facile Re–^{16}O–Zr → Re–^{18}O–Zr substitution is evidenced for the anchoring site, justified by the isotopic shift undergone by the ~885 cm⁻¹ Re–O–Zr band already from the 1st $^{18}O/^{16}O$ cycle.

For both 1.3ReZrO₂ and 2.4ReZrO₂ samples with coverages of 1.3 and 2.4 Re nm⁻², the di-oxo Species-IIa prevails at 400 °C, whilst the mono-oxo Species-I and the di-oxo Species-IIb also exist in minority. The pertinent isotopic effects observed are similar for the two samples and differ from the ones observed for 0.71ReZrO₂ only due to the different speciation of the dispersed ReO_x phase. More specifically:

(i) A facile Re–^{16}O–Zr → Re–^{18}O–Zr substitution is evidenced already after the 1st $^{18}O/^{16}O$ cycle (and largely after the fifth cycle), justified by the isotopic shift undergone by the ~888 cm⁻¹ Re–O–Zr mode.

(ii) The bands emerging due to $(Re{=}^{18}O)_n$ at 942 cm⁻¹ for 1.3ReZrO₂ (Fig. 9B) and 946 cm⁻¹ for 2.4ReZrO₂ (Fig. 9C) exhibit in each case a shoulder on their low wavenumber wing in the initial stages of the isotopic exchange clearly seen after the 1st cycle at 936 cm⁻¹ for 1.3ReZrO₂ (Fig. 9B) and 940 cm⁻¹ for 2.4ReZrO₂ (Fig. 9C), thereby indicating a facile $^{16}O{=}Re{=}^{16}O$ → $^{18}O{=}Re{=}^{18}O$ substitution for the minority di-oxo Species–IIb. With further progress in the $^{18}O/^{16}O$ substi-
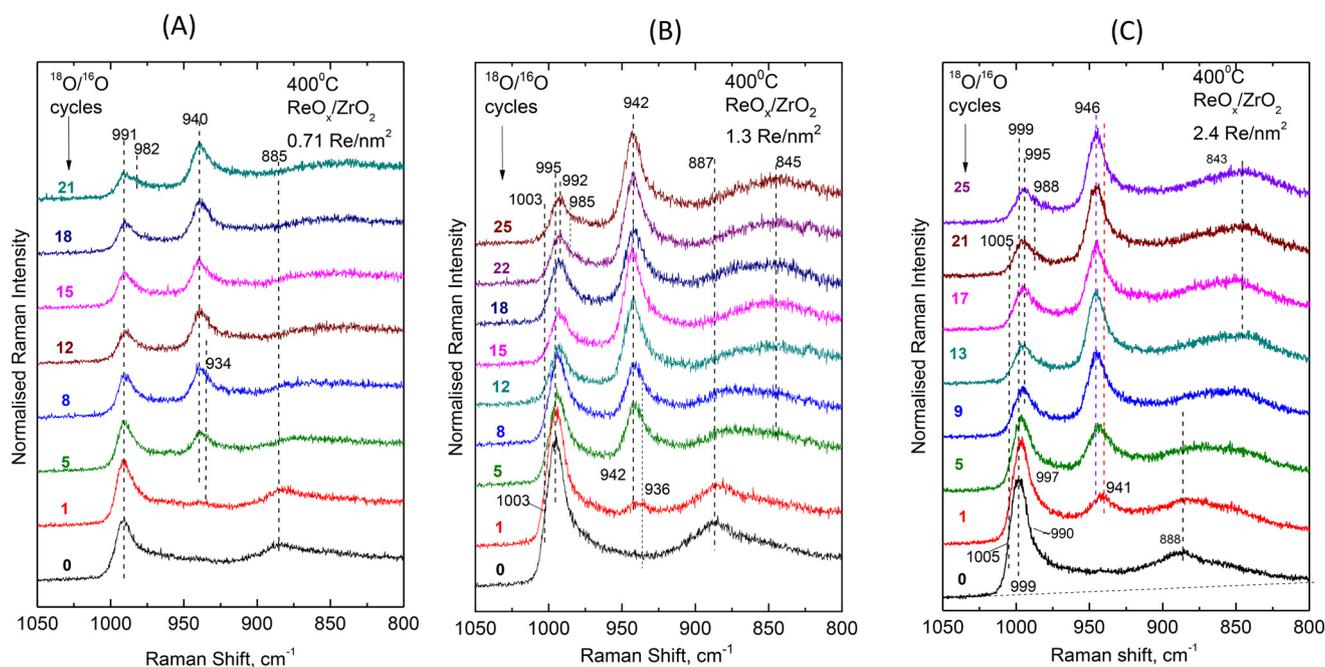
Fig. 9 Sequential *in situ* Raman spectra obtained at 400 °C under flowing 2% $^{18}O_2$/He after subsequent $H_2/^{18}O_2$ reduction/oxidation cycles as indicated by each spectrum. (A) ReO_x/ZrO₂ with surface density of 0.71 Re nm⁻²; (B) ReO_x/ZrO₂ with surface density of 1.3 V nm⁻²; and (C) ReO_x/ZrO₂ with surface density of 2.4 Re nm⁻²; spectral recording parameters: see Fig. 2 caption.

tution the main bands' masses due to the prevailing Species-IIa at 942 and 946 cm^{-1} obscure the shoulders.

(iii) After 25 ^{18}O/^{16}O substitution cycles the band envelope due to the non-substituted (Re=^{16}O)$_n$ modes appears red-shifted (995 → 992 cm^{-1} for 1.3 ReZrO$_2$, Fig. 9B and 999 → 995 cm^{-1} for 2.4 ReZrO$_2$, Fig. 9C) due to the earlier described[28,30] next-nearest-neighbor vibrational isotope effect caused by the facile Re–^{16}O–Zr → Re–^{18}O–Zr substitution on the anchoring sites. Moreover, the convolutions of the 992 and 995 cm^{-1} bands due to the non-substituted (Re=^{16}O)$_n$ modes after 25 cycles possess each a low wavenumber shoulder (at 985 and 988 cm^{-1}, respectively for 1.3ReZrO$_2$ and 2.4ReZrO$_2$), assigned to partially substituted ^{18}O=Re=^{16}O sites.[16,20,21,43]

(iv) The Re=^{16}O modes due to the mono-oxo Species-I at 1003 cm^{-1} (1.3ReZrO$_2$, Fig. 9B) and at 1005 cm^{-1} (2.4ReZrO$_2$, Fig. 9C) are entirely diminished after 8 and 9 ^{18}O/^{16}O cycles, confirming a facile Re=^{16}O → Re=^{18}O substitution for the mono-oxo Species-I.

3.3. Synopsis of structural interpretations

In the temperature range of 120–400 °C, the (ReO$_x$)$_n$ phase dispersed on ZrO$_2$ is built of three main structural units, namely mono-oxo Species-I, di-oxo Species-IIa and di-oxo Species-IIb. At low coverage of n_s = 0.71 Re nm^{-2} most ReO$_x$ sites are isolated on ZrO$_2$. At higher coverages of $n_s \geq 1.3$ Re nm^{-2}, the occurrence of ReO$_x$ in vicinal sites may favor the formation of associated species by means of Re–O–Re linkages. Hence, with increasing loading, a lowering of the Raman band intensity due to Re–O–Zr at ~885–890 cm^{-1} relative to Re(=O)$_n$ (n = 1, 2 for mono-oxo and di-oxo species, respectively) at 991–1003 cm^{-1} is observed (Fig. 2A–C) and a concomitant increase of a partly obscured broad feature at ~935–940 cm^{-1} (Fig. 2A–C) that has previously also been assigned as due to bridging modes (Re–O–Re or O–Re–O).[44]

A reversible temperature-dependent interconversion is evidenced between mono-oxo Species–I and di-oxo Species–IIa mediated by water molecules retained at the surface layer according to reaction scheme (A), portrayed also in Fig. 8. The Species-IIa → Species-I transformation taking place with increasing temperature requires the occurrence of two OH sites adjacent to a Species-IIa. Such a mechanism is limited at coverages of $n_s \geq 1.3$ Re nm^{-2} as seen in Fig. 7B and C due to larger extent of preceded titration of surface hydroxyls, thereby limiting the availability of surface hydroxyls and lowering of the possibility for occurrence of two surface hydroxyls adjacent to each Species-IIa.

As discussed, the Species–IIb di-oxo structural unit does not undergo transformations in the temperature range of 120–400 °C and its presence remains stable, as seen in Fig. 7 (A–C). However, as seen *e.g.* in Fig. S3(A)† pertaining to the low coverage 0.71ReZrO$_2$ sample, there is evidence for a temperature-dependent reversible Species-IIb ↔ Species-III interconversion. Species-III is represented by a main Re(=O)$_n$ stretching band at ~974 cm^{-1} (see spectrum (a) in Fig. S3(A)† pertaining to 35 °C), of which the appearance is observed with decreasing temperature together with a concomitant diminish-
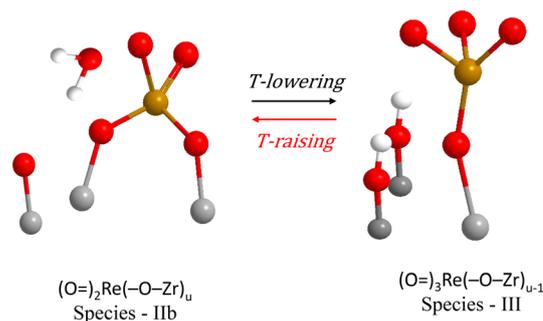
Fig. 10 Molecular-level mechanism accounting for the reversible temperature-dependent Species-IIb ↔ Species-III transformation mediated by water molecules retained at the surface layer and surface hydroxyls. For simplicity, mononuclear representations are shown. The number of anchoring bonds and the resulting coordination number, CN$_{Re}$ = 4 are reasonable in view of the oxidation state VII for Re and the tri-oxo termination configuration of Species-III. Gold spheres, Re; red spheres, O; grey spheres, Zr. H atoms (white spheres) are included to account for hydroxylation (see text).

ing of the ~885 cm^{-1} Re–O–Zr band. Hence, the ~974 cm^{-1} band is assigned to an isolated tri-oxo site possessing less Re–O–Zr anchors, formed according to the scheme:

$$\underset{\text{Species–IIb}}{(O{=})_2 Re(-O-Zr)_u} + HOH + (Zr-O-)$$

$$\underset{\text{T-raising}}{\overset{\text{T-lowering}}{\rightleftharpoons}} \underset{\text{Species–III}}{(O{=})_3 Re(-O-Zr)_{u-1}} + Zr-OH + Zr-OH \qquad \text{(B)}$$
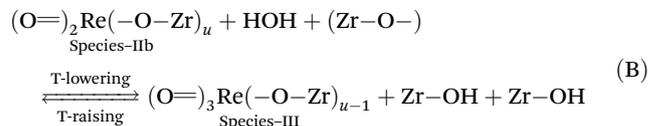
Fig. 10 shows a molecular-level mechanism accounting for the above reaction scheme (B). The occurrence of tri-oxo Species-III units is not favored at coverages of $n_s \geq 1.3$ Re nm^{-2} where associated species possessing Re–O–Re linkages prevail.

Finally, apart from the temperature and coverage effects, it is noteworthy to also address in synopsis the most recently reported and well-documented effects of metal oxide carrier type on the speciation of the ReO$_x$ dispersed phase. Significantly, the heterogeneity of the dispersed phase is hitherto established also for ReO$_x$ deposited on Al$_2$O$_3$,[16] TiO$_2$[20] and CeO$_2$.[21] In particular, the existence of two di-oxo species has been proposed for ReO$_x$/Al$_2$O$_3$ catalysts,[16] whilst the occurrence of a mono-oxo and a di-oxo species has been evidenced for ReO$_x$/TiO$_2$[20] and ReO$_x$/CeO$_2$[21] catalysts. To the contrary, one single ReO$_x$ species taking on a tri-oxo configuration was found for ReO$_x$/SiO$_2$.[17]

4. Conclusions

In situ molecular spectroscopy is used for studying the vibrational properties and unravelling the structural and configurational characteristics of the (ReO$_x$)$_n$ phase dispersed on monoclinic ZrO$_2$. *In situ* Raman and *in situ* FTIR spectra (the former also coupled with ^{18}O/^{16}O exchange) are exploited under dehydrated feed conditions, covering a surface density span of 0.71–3.7 Re nm^{-2}.

(a) The $(ReO_x)_n$ phase dispersed on ZrO_2 is heterogeneous, consisting of distinct structural units. In the temperature range of 120–400 °C, three main structural units are identified: (i) Species–I with mono-oxo termination configuration, $O=$ $(Re–O–Zr)_m$; (ii) Species–IIa with di-oxo termination configuration, $(O=)_2(Re–O–Zr)_{m-1}$; and (iii) Species–IIb with di-oxo termination configuration, $(O=)_2(Re–O–Zr)_u$.

(b) At low coverage of 0.71 Re nm^{-2}, isolated (monomeric) ReO_x species prevail. At 400 °C, the mono-oxo Species-I predominates, Species-IIa is significantly present, whilst Species-IIb occurs in minority.

(c) A reversible temperature-dependent Species-I $\leftrightarrow$ Species-IIa transformation is evidenced, shifting to the right with decreasing temperature.

(d) At coverages of $n_s \geq 1.3$ Re nm^{-2}, Species-IIa clearly prevails over Species-I, in the full temperature range of 120–400 °C.

(e) The terminal stretching wavenumbers of all Species undergo a blue shift with increasing coverage, presumably due to variations in the basicity of dative O support atoms and/or vibrational coupling in associated $(ReO_x)_n$ moieties. As an example, at 400 °C, the terminal Re$=$O stretching mode for Species-I is found at 993–1005 cm^{-1}, the symmetric stretching mode for Species-IIa is found at 987–998 cm^{-1} and the counterpart symmetric stretching mode for Species-IIb at 982–991 cm^{-1}.

(f) At temperature below 80 °C and for a low coverage of 0.71 Re nm^{-2}, the occurrence of a fourth structural unit Species-III is evidenced, taking on a tri-oxo termination configuration with a symmetric stretching mode at 974 cm^{-1}.

(g) The isotopic $^{18}O/^{16}O$ substitution experiments show a facile Re–^{16}O–Zr $\rightarrow$ Re–^{18}O–Zr substitution and a relative ease for $(^{16}O=)_2(Re–O–Zr)_u \rightarrow (^{18}O=)_2(Re–O–Zr)_u$ substitution for the minority Species-IIb.

(h) All temperature-dependent changes and structural transformations are fully reversible under dehydrated feed conditions.

(i) It is feasible to tune the speciation of the $(ReO_x)_n$ phase dispersed on ZrO_2 by suitably controlling the temperature and the coverage.

Conflicts of interest

There are no conflicts to declare.

Acknowledgements

References

1 J. A. Moulijn and J. C. Mol, Structure and Activity of Rhenium-Based Metathesis Catalysts, *J. Mol. Catal.*, 1988, **46**, 1–14.

2 J. C. Mol, Olefin Metathesis over Supported Rhenium Oxide Catalysts, *Catal. Today*, 1999, **51**, 289–299.

3 S. Lwin and I. E. Wachs, Olefin Metathesis by Supported Metal Oxide Catalysts, *ACS Catal.*, 2014, **4**, 2505–2520.

4 C.-B. Wang, Y. Cai and I. E. Wachs, Reaction-Induced Spreading of Metal Oxides onto Surfaces of Oxide Supports During Alcohol Oxidation: Phenomenon, Nature, and Mechanisms, *Langmuir*, 1999, **15**, 223–1235.

5 Y. Yuan, T. Shido and Y. Iwasawa, The New Catalytic Property of Supported Rhenium Oxides for Selective Oxidation of Methanol to Methylal, *Chem. Commun.*, 2000, 1421–1422.

6 Y. Yuan, K. Tsai, H. Liu and Y. Iwasawa, Selective Methanol Conversion to Methylal on Re-Sb-O Crystalline Catalysts: Catalytic Properties and Structural Behavior, *Top. Catal.*, 2003, **22**, 9–15.

7 X. Secordel, E. Berier, M. Capron, S. Cristol, J.-F. Paul, M. Fournier and E. Payen, TiO$_2$-Supported Rhenium Oxide Catalysts for Methanol Oxidation: Effect of Support Texture on The Structure and Reactivity Evidenced by an Operando Raman Study, *Catal. Today*, 2010, **155**, 177–183.

8 A. Yoboue, A. Susset, A. Tougerti, D. Gallego, S. V. Ramani, M. Kalyanikar, D. S. Dolzhnikov, S. G. Wubshet, Y. Wang, S. Cristol, V. Briois, C. La Fontaine, R. M. Gauvin, J.-F. Paul and E. Berier, An Easily Accessible Re-Based Catalyst for the Selective Conversion of Methanol: Evidence for an Unprecedented Active Site Structure Through Combined Operando Techniques, *Chem. Commun.*, 2011, **47**, 4285–4287.

9 R. Thomas, E. M. van Oers, V. H. J. de Beer, J. Medema and J. A. Moulijn, Characterization of γ-alumina-supported Molybdenum Oxide and Tungsten Oxide; Reducibility of the Oxidic State Versus Hydrodesulfurization Activity of the Sulfided State, *J. Catal.*, 1982, **76**, 241–253.

10 N. Escalona, J. Ojeda, R. Cid, G. Alves, A. L. Agudo, J. L. G. Fierro and F. J. G. Llambias, Characterization and Reactivity of Re(x)/γ-Al$_2$O$_3$ Catalysts in Hydrodesulfurization and Hydrodenitrogenation of Gas Oil: Effect of Re Loading, *Appl. Catal., A*, 2002, **234**, 45–54.

11 M. Vuurman, D. J. Stufkens, A. Oskam and I. E. Wachs, Structural determination of surface rhenium oxide on various oxide supports (Al$_2$O$_3$, ZrO$_2$, TiO$_2$ and SiO$_2$), *J. Mol. Catal.*, 1992, **76**, 263–285.

12 D. S. Kim and I. E. Wachs, Surface Rhenium Oxide-Support Interaction for Supported Re$_2$O$_7$ Catalysts, *J. Catal.*, 1993, **141**, 419–429.

13 B. Mitra, X. Gao, I. E. Wachs, A. M. Hirt and G. Deo, Characterization of Supported Rhenium Oxide Catalysts: Effect of Loading, Support and Additives, *Phys. Chem. Chem. Phys.*, 2001, **3**, 1144–1152.

14 B. M. Weckhuysen, J.-M. Jehng and I. E. Wachs, In Situ Raman Spectroscopy of Supported Transition Metal Oxide Catalysts: $^{18}O_2$-$^{16}O_2$ Isotopic Labeling Studies, *J. Phys. Chem. B*, 2000, **104**, 7382–7387.

15 S. R. Bare, S. D. Kelly, F. D. Vila, E. Boldingh, E. Karapetrova, J. Kas, G. E. Mickelson, F. S. Modica, N. Yang and J. J. Rehr, Experimental (XAS, STEM, TPR, and XPS) and Theoretical (DFT) Characterization of Supported Rhenium Catalysts, *J. Phys. Chem. C*, 2007, **111**, 5740–5745.

16 S. Lwin, C. Keturakis, J. Handzlik, P. Sautet, Y. Li, A. I. Frenkel and I. E. Wachs, Surface ReO_x Sites on Al_2O_3 and their Molecular Structure-Reactivity Relationships for Olefin Metathesis, *ACS Catal.*, 2015, **5**, 1432–1444.

17 E. L. Lee and I. E. Wachs, In Situ Raman Spectroscopy of SiO_2-Supported Transition Metal Oxide Catalysts: An Isotopic ^{18}O–^{16}O Exchange Study, *J. Phys. Chem. C*, 2008, **112**, 6487–6498.

18 C. Andriopoulou and S. Boghosian, Heterogeneity of Deposited Phases in Supported Transition Metal Oxide Catalysts: Reversible Temperature-Dependent Evolution of Molecular Structures and Configurations, *Phys. Chem. Chem. Phys.*, 2018, **20**, 1742–1751.

19 C. Andriopoulou and S. Boghosian, Tuning the Configuration of Dispersed Oxometallic Sites in Supported Transition Metal Oxide Catalysts: A Temperature Dependent Raman Study, *Catal. Today*, 2019, **336**, 74–83.

20 C. Andriopoulou and S. Boghosian, Molecular Structure and Termination Configuration of Oxo-Re(vii) Catalyst Sites Supported on Titania, *Catal. Today*, 2020, **355**, 665–677.

21 B. MacQueen, B. Ruiz-Yi, M. Royko, A. Heyden, Y. J. Pagan-Torres, C. Williams and J. Lauterbach, *In situ* Oxygen Isotopic Exchange Vibrational Spectroscopy of Rhenium Oxide Surface Structures on Cerium Oxide, *J. Phys. Chem. C*, 2020, **124**, 7174–7181.

22 J. Strunk, M. A. Banares and I. E. Wachs, Vibrational Spectroscopy of Oxide Overlayers, *Top. Catal.*, 2017, **60**, 1577–1617.

23 Th. Kentri, A. Trimpalis, A. Misa, E. Kordouli, Th. Ramantani and S. Boghosian, Rethinking Molecular Structures of $W^{vi}O_x$ Sites Dispersed on Titania. Distinct Mono-Oxo Configurations at 430 °C and Temperature-Dependent Transformations, *Dalton Trans.*, 2022, **51**, 7455–7475.

24 Th. Kentri, A. Tsevis and S. Boghosian, Heterogeneity of the vanadia phase dispersed on titania. Co-existence of distinct mono-oxo VO_x sites, *Dalton Trans.*, 2023, **52**, 7495–7511.

25 K. Nakamoto, *Infrared and Raman Spectra of Inorganic and Coordination Compounds*, Wiley – Interscience, New York, 6th edn, 2009.

26 C. Andriopoulou, I. Anastasiou and S. Boghosian, Di-Oxo and Tri-Oxo Re(vii)-Oxosulfato Complexes in the Re_2O_7-

$K_2S_2O_7$ Molten System. Molecular Structure, Vibrational Properties and Temperature-Dependent Interconversion, *Vib. Spectrosc.*, 2019, **100**, 14–21.

27 A. Christodoulakis and S. Boghosian, Molecular Structure and Activity of Molybdena Catalysts Supported on Zirconia for Ethane Oxidative Dehydrogenation Studied by Operando Raman Spectroscopy, *J. Catal.*, 2008, **260**, 178–187.

28 G. Tsilomelekis and S. Boghosian, On the Configuration, Molecular Structure and Vibrational Properties of MoO_x Sites on Alumina, Zirconia, Titania and Silica, *Catal. Sci. Technol.*, 2013, **3**, 1869–1888.

29 C. Andriopoulou, D. Harris, H. Stephenson, A. M. Eftsathiou and S. Boghosian, In situ Raman Spectroscopy as a Tool for Discerning Subtle Structural Differences Between Commercial $(Ce,Zr)O_2$-Based OSC Materials of Identical Composition, *Catalysts*, 2020, **10**, 462.

30 G. Tsilomelekis and S. Boghosian, In Situ Raman and FTIR Spectroscopy of Molybdenum(vi) Oxide Supported on Titania Combined with $^{18}O/^{16}O$ Exchange: Molecular Structure, Vibrational Properties and Vibrational Isotope Effects, *J. Phys. Chem. C*, 2011, **118**, 2146–2154.

31 G. Tsilomelekis and S. Boghosian, Structural and Vibrational Properties of Molybdena Catalysts Supported on Alumina and Zirconia Studied by in Situ Raman and FTIR Spectroscopies Combined with $^{18}O/^{16}O$ Isotopic Substitution, *Catal. Today*, 2010, **158**, 146–155.

32 K. Bourikas, K. Ch. Kordulis and A. Lycourghiotis, Titanium Dioxide (Anatase and Rutile): Surface Chemistry, Liquid–Solid Interface Chemistry, and Scientific Synthesis of Supported Catalysts, *Chem. Rev.*, 2014, **114**, 9754–9823.

33 G. D. Panagiotou, Th. Petsi, K. Bourikas, Ch. Kordulis and A. Lycourghiotis, The Interfacial Impregnation Step Involved in the Preparation of Tungsten(vi) Supported Titania Catalysts, *J. Catal.*, 2009, **262**, 266–279.

34 G. D. Panagiotou, Th. Petsi, K. Bourikas, A. G. Kalampounias, S. Boghosian, Ch. Kordulis and A. Lycourghiotis, Interfacial Impregnation Chemistry in the Synthesis of Molybdenum Catalysts Supported on Titania, *J. Phys. Chem. C*, 2010, **114**, 11868–11879.

35 G. Tsilomelekis, G. D. Panagiotou, P. Stathi, A. G. Kalampounias, K. Bourikas, Ch. Kordulis, Y. Deligiannakis, S. Boghosian and A. Lycourghiotis, Molybdena Deposited on Titania by Equilibrium Deposition Filtration: Structural Evolution of Oxo–Molybdenum(vi) Sites with Temperature, *Phys. Chem. Chem. Phys.*, 2016, **18**, 23980–23989.

36 A. Tribalis, G. D. Panagiotou, G. Tsilomelekis, A. G. Kalampounias, K. Bourikas, Ch. Kordulis, S. Boghosian and A. Lycourghiotis, Temperature-Dependent Evolution of the Molecular Configuration of Oxo-Tungsten(vi) Species Deposited on the Surface of Titania, *J. Phys. Chem. C*, 2014, **118**, 11319–11332.

37 E. Tella, A. Trimpalis, A. Tsevis, Ch. Kordulis, A. Lycourghiotis, S. Boghosian and K. Bourikas, Advanced

Synthesis and Characterization of Vanadia/Titania Catalysts Through a Molecular Approach, *Catalysts*, 2021, **11**, 322.

38 S. Loridant, C. Feche, N. Essayem and F. Figueras, WO_x/ZrO_2 Catalysts Prepared by Anionic Exchange; In situ Raman Investigation from the Precursor Solutions to the Calcined Catalysts, *J. Phys. Chem. B*, 2005, **109**, 5631–5637.

39 B.-K. Kim and H. Hamaguchi, Mode Assignments of the Raman Spectrum of Monoclinic Zirconia by Isotopic Exchange Technique, *Phys. Status Solidi B*, 1997, **203**, 557–563.

40 G. Herzberg, *Molecular Spectra and Molecular Structure, I. Spectra of Diatomic Molecules*, Van Nostrand Company Inc., Princeton, 2nd edn, 1950.

41 G. Busca, Differentiation of Mono-oxo and Polyoxo and of Monomeric and Polymeric Vanadate, Molybdate and Tungstate Species in Metal Oxide Catalysts by IR and Raman Spectroscopy, *J. Raman Spectrosc.*, 2002, **33**, 348–358.

42 G. Herzberg, *Molecular Spectra and Molecular Structure, II. Infrared and Raman Spectra of Polyatomic Molecules*, Van Nostrand Company Inc., Princeton, 2nd edn, 1950.

43 S. Chempath, Y. Zhang and A. T. Bell, DFT Studies of the Structure and Vibrational Specttra of Isolated Molybdena Species Supported on Silica, *J. Phys. Chem. C*, 2007, **111**, 1291–1298.

44 M. A. Banares and I. E. Wachs, Raman Spectroscopy of Catalysts, in *Encyclopedia of Analytical Chemistry*, 2010, John Wiley & Sons, pp. 1–30.